

The symmetry of charge order in cuprates

R. Comin,^{1,*} R. Sutarto,² F. He,² E. da Silva Neto,^{1,3,4} L. Chauviere,^{1,3,4} A. Frano,^{4,5} R. Liang,^{1,3} W.N. Hardy,^{1,3} D.A. Bonn,^{1,3} Y. Yoshida,⁶ H. Eisaki,⁶ J. E. Hoffman,⁷ B. Keimer,⁴ G.A. Sawatzky,^{1,3} and A. Damascelli^{1,3,†}

¹*Department of Physics & Astronomy, University of British Columbia, Vancouver, British Columbia V6T 1Z1, Canada*

²*Canadian Light Source, University of Saskatchewan, Saskatoon, Saskatchewan S7N 0X4, Canada*

³*Quantum Matter Institute, University of British Columbia, Vancouver, British Columbia V6T 1Z4, Canada*

⁴*Max Planck Institute for Solid State Research, Heisenbergstrasse 1, D-70569 Stuttgart, Germany*

⁵*Helmholtz-Zentrum Berlin für Materialien und Energie, Wilhelm-Conrad-Röntgen-Campus BESSY II, Berlin, Germany*

⁶*National Institute of Advanced Industrial Science and Technology (AIST), Tsukuba, 305-8568, Japan*

⁷*Department of Physics, Harvard University, Cambridge, MA 02138, U.S.A.*

(Dated: March 5, 2014)

Charge-ordered ground states permeate the phenomenology of $3d$ -based transition metal oxides, and more generally represent a distinctive hallmark of strongly-correlated states of matter. The recent discovery of charge order in various cuprate families fueled new interest into the role played by this incipient broken symmetry within the complex phase diagram of high- T_c superconductors. Unveiling its origin and nature is key to a microscopic understanding of the normal state, which carries the seeds of unconventional superconductivity. Here we use resonant X-ray scattering to resolve the main characteristics of the charge-modulated state in two cuprate families: $\text{Bi}_2\text{Sr}_{2-x}\text{La}_x\text{CuO}_{6+\delta}$ (Bi2201) and $\text{YBa}_2\text{Cu}_3\text{O}_{6+y}$ (YBCO). As a first result, we detect no signatures of spatial modulations along the nodal direction in Bi2201, thus clarifying the *inter-unit-cell* momentum-structure of the order parameter. In addition, by adopting a special experimental geometry, we also resolve the *intra-unit-cell* symmetry of the charge ordered state, which is revealed to be predominantly a d -wave bond-order with modulated charges on the O- $2p$ orbitals. These results represent a fundamental advancement in our microscopic description of charge order in cuprates, and provide crucial insights for the understanding of its origin and interplay with superconductivity and magnetism.

Complex oxides exhibit a mosaic of exotic electronic phases with various symmetry-broken ground states that revolve around three main instabilities: antiferromagnetism, charge order, and superconductivity. In particular, charge order – the tendency of the valence electrons to segregate in periodically-modulated structures – is found in various classes of strongly-correlated $3d$ -oxides, such as manganites [1], nickelates [2], and cobaltates [3]. The original discovery of period-4 stripe-like charge correlations in the La-based materials [4–7] confirmed the central role played by charge-ordered states in the physics of underdoped cuprates, as anticipated by earlier theoretical work [8–11]. Following further indications by surface-sensitive scanning tunnelling microscopy (STM) [12, 13], the field was recently revived by the detection of charge-modulated states with wavevector $Q^* \sim 0.31$ reciprocal lattice units (r.l.u., used hereafter) in YBCO using nuclear magnetic resonance [14] and resonant elastic/inelastic X-ray scattering (REXS/RIXS) [15–20]. Even more recently, this phenomenology was confirmed in Bi-based materials (with $Q^* \sim 0.26$ and 0.3 in single- and double-layer compounds, respectively), as observed in both bulk/momentum space (with REXS) and surface/real space (with STM) [21, 22]. These multiple experimental observations establish a ubiquitous instability toward charge ordering in the underdoped region of the phase diagram.

The microscopic mechanisms that lead to charge order, and govern its interplay with superconductivity and magnetism, are key to the ultimate understanding of the

multiple electronic phases that emerge out of the interaction between charge, spin, and lattice degrees of freedom. The relevance of this electronic instability has been extensively pointed out [23] and recently resurged as a prominent topic [24–34], sparking an intense debate and urging the need for further experimental investigations of the microscopic structure of the charge-ordered state. Several important questions – such as where charges reside and what is their local symmetry – remained unanswered to date, partly due to the lack of a tailored experimental scheme to probe these subtle but fundamental details.

Here we explore the detailed momentum structure of the charge-density-wave (CDW) order parameter $\Delta_{\text{CDW}}(\mathbf{k}, \mathbf{Q})$ using REXS, which probes the electronic density directly in reciprocal space, with extreme sensitivity. Our study addresses two major open questions: (i) whether CDW signatures in (Q_x, Q_y) space are found exclusively along the antinodal directions at $(Q^*, 0)$ and $(0, Q^*)$, or whether they are also present along the nodal axis at (Q^*, Q^*) , as discussed in [24, 25, 28, 29, 31–33]; (ii) how are charges distributed spatially, and what is the resulting local symmetry of the ordered state [24–27, 33, 34]. In more general terms, points (i) and (ii) relate to the \mathbf{Q} - (*inter-unit-cell*) and \mathbf{k} - (*intra-unit-cell*) dependence of the order parameter, respectively.

The first part of this work, aimed at addressing the \mathbf{Q} -structure of Δ_{CDW} , was performed on the underdoped single-layer compound $\text{Bi}_2\text{Sr}_{1.2}\text{La}_{0.8}\text{CuO}_{6+\delta}$ (Bi2201-UD15K), with hole doping $p \sim 0.11$ and $T_c =$

15 K. This material exhibits signatures of incommensurate CDW with wavevector $(Q^*, 0) = (0.265, 0)$ [21]. The smaller value of Q^* allows reaching – at the Cu- L_3 edge – momenta located near (Q^*, Q^*) which in contrast are *not* accessible in double-layer YBCO and $\text{Bi}_2\text{Sr}_2\text{CaCu}_2\text{O}_{8+\delta}$. We use REXS to selectively probe the CuO_2 -derived electronic states by tuning the photon energy to the Cu- L_3 absorption resonance. The corresponding experimental results for the momentum-resolved electronic density in the CuO_2 planes are shown in Fig. 1a for the two high-symmetry directions $(H, 0)$ and (H, H) in the (Q_x, Q_y) plane. The REXS data are consistent with the real-space maps of the electronic density obtained by STM, whose $(H, 0)$ and (H, H) cuts in Fourier (\mathbf{Q}) space are shown in Fig. 1b (Fourier-transformed STM, STM-FT). Due to the presence of charge order peaks both along $(H, 0)$ and $(0, H)$, the experimental data are compatible with both

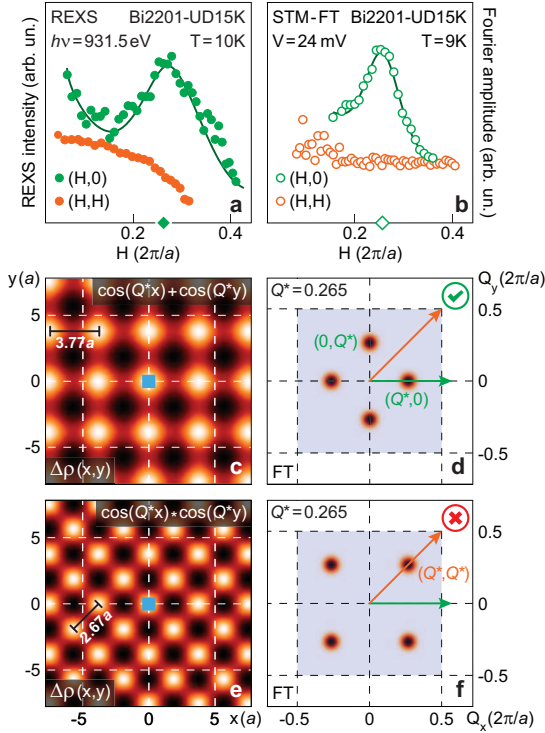


FIG. 1: **a,b**, Low-temperature REXS (at photon energy $h\nu = 931.5$ eV) and Fourier-transformed (FT) STM scans (at constant bias voltage $V = 24$ mV), respectively, from an underdoped Bi2201-UD15K sample, mapping reciprocal-space features along the two high-symmetry directions: $(H, 0)$, antinodal, green; and (H, H) , nodal, orange. **c,e**, Modulation of the charge density $\Delta\rho(x, y)$, with functional form given by a sum (c) and product (e) of cosines, and a wavevector magnitude $Q^* = 0.265$ r.l.u. (black bars indicate the period and direction of the spatial modulation, expressed in terms of the lattice parameter $a = 3.86$ Å). The blue rectangles denote the undistorted unit cell. **d,f**, Fourier transforms of **c,e**, with Gaussian broadening. The arrows indicate the directions of the data in **a,b**, which validate the scenario in **c,d**.

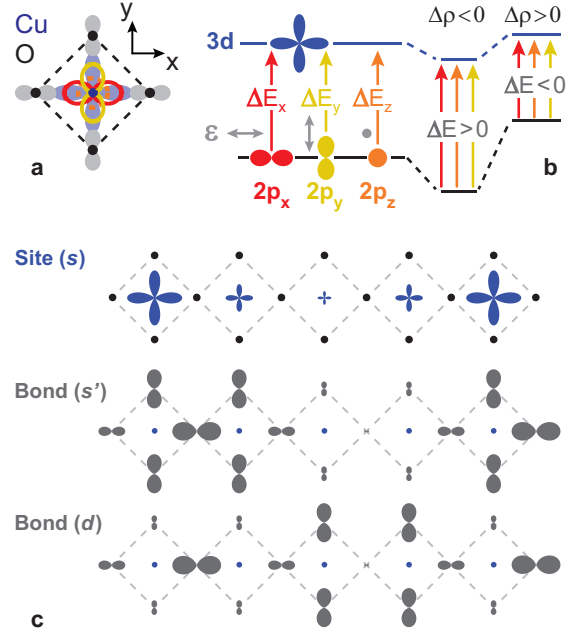


FIG. 2: **a**, Low-energy orbitals in a single CuO_4 plaquette (the orbital size is not proportional to the actual mean-squared radius). **b**, REXS excitation channels at the Cu- $L_{2,3}$ edge; ϵ denotes light polarization (gray arrows), here used to control which Cu- $2p$ core electron is photoexcited into a Cu- $3d$ state. A varying density modulates the orbital energies, and consequently the transition energies $\Delta E_{x,y,z}(\mathbf{r})$. **c**, Real-space schematics of the periodically-modulated density $\Delta\rho$ in the case of site-order (charges on Cu), or bond-order (charges on O) with either extended s -wave or d -wave local symmetry (top to bottom), along a single crystallographic direction.

checkerboard order (bidirectional) or alternating stripes (unidirectional). In the case of bidirectional order, the two simplest modulation patterns of the charge density $\Delta\rho(x, y)$ with wavevector $Q^* = 0.265$ (r.l.u.) are given by: (i) $\Delta\rho(x, y) = \cos(Q^*x) + \cos(Q^*y)$ (Fig. 1c); and (ii) $\Delta\rho(x, y) = \cos(Q^*x) \times \cos(Q^*y)$ (Fig. 1e). Case (i) corresponds to reciprocal space features along the $(H, 0)$ and $(0, H)$ axes (Fig. 1d), whereas (ii) yields spatial frequencies along the (H, H) and $(H, -H)$ direction (Fig. 1f). Since no CDW peaks are observed along (H, H) in both the REXS and STM data, we conclude that the scenario (ii) can be ruled out, thus establishing that charge modulations exclusively run parallel to the Cu-O bond directions (**a** and **b** axes).

The second and main part of this study focuses on the \mathbf{k} -structure of the CDW order parameter, which controls the local arrangement of excess charges within each CuO_4 plaquette. REXS is able to probe the local charge density $\Delta\rho(\mathbf{r})$ through the spatial modulation of the core-to-valence transition energies $\Delta E(\mathbf{r})$ [17, 35]. The latter correspond to the energy difference between the core (Cu- $2p$) and valence (Cu- $3d$) orbitals involved in the scattering process, which are modulated in pres-

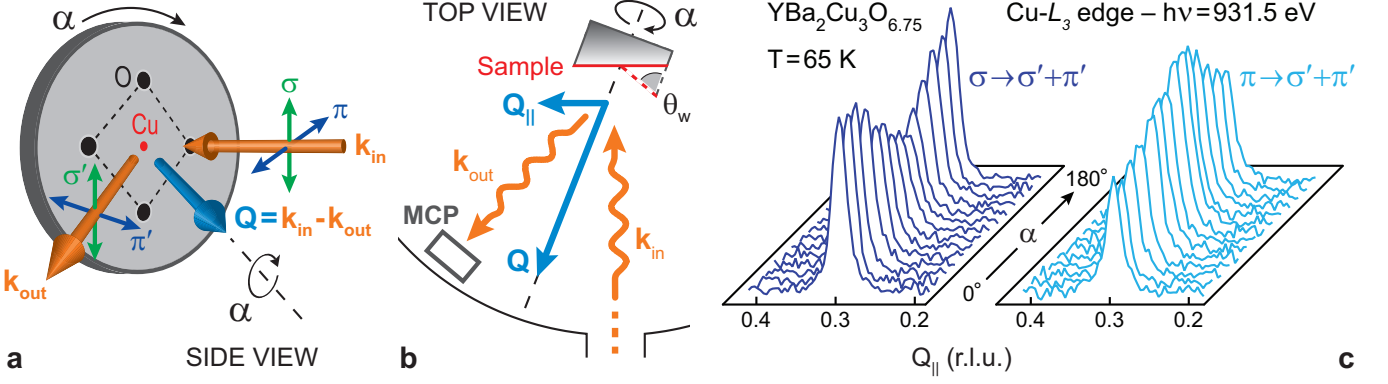


FIG. 3: **a**, Side view of the experimental geometry; control variables are: (i) the incoming and outgoing photon wavevectors \mathbf{k}_{in} and \mathbf{k}_{out} , which determine the exchanged momentum \mathbf{Q} ; (ii) the incoming (linear) polarization ϵ_{in} ($=\sigma$ or π); (iii) the azimuthal angle α , whose rotation axis $\hat{\mathbf{u}}_{\alpha}$ coincides with the direction of \mathbf{Q} . The polarization of scattered x-rays (σ' or π') is not analyzed. **b**, Top view, illustrating the need for a wedge-shaped sample holder to guarantee the condition $\hat{\mathbf{u}}_{\alpha} \parallel \mathbf{Q}$ for the specific \mathbf{Q} -vector of interest ($\theta_w = 67.5^\circ$ and 72° for YBCO and Bi2201, respectively). Scattered photons are collected using a multi-channel-plate (MCP) detector. **c**, Azimuthal angle-dependent \mathbf{Q} -scans of the CDW peak (after subtraction of fluorescence background) at $\mathbf{Q}_{\text{CDW}} = (0, 0.31, 1.5)$ in YBCO-OrthoIII, plotted vs. the CuO_2 -plane projection of the exchanged momentum Q_{\parallel} .

ence of a spatially-varying electronic density through the Coulomb interaction [24] (see Fig. 2a,b and Supplementary Information). In order to evaluate the symmetry of the CDW order parameter Δ_{CDW} , we can selectively probe the different transition channels ($\text{Cu-}2p_{x,y,z} \rightarrow 3d$) by rotating the light polarization in the REXS measurements. Here we focus on three possibilities for Δ_{CDW} : (i) a site-centered modulation ($\Delta_{\text{CDW}} = \Delta_s$), corresponding to an extra charge residing on the Cu-3d orbital (Fig. 2c, top); (ii) an extended s -wave bond-order [$\Delta_{\text{CDW}} = \Delta_{s'}(\cos k_x + \cos k_y)$], where the spatially-modulated density is on the O-2p states, and the maxima along the x and y directions coincide (Fig. 2c, middle); (iii) a d -wave bond-order [$\Delta_{\text{CDW}} = \Delta_d(\cos k_x - \cos k_y)$], where the charge modulation changes sign between x- and y-coordinated oxygen atoms, and the maxima are shifted by a half wavelength (Fig. 2c, bottom). The resulting shifts of orbital energies and corresponding transition energies ($\Delta E_{x,y,z}$) at the Cu- L_3 edge have been calculated using a peak-to-trough charge amplitude of $0.1e$, as suggested by STM [21, 36] studies.

In the experiments we use a special geometry, in which the sample is rotated around the ordering vector \mathbf{Q}^* (Fig. 3a,b). This method allows looking at the same wavevector while modulating (as a function of the azimuthal rotation angle α) the relative weight of the Cu $2p_{x,y,z} \rightarrow 3d$ transitions, which is controlled by the light polarization through dipole selection rules (see Fig. 2b and Supplementary Table I). Here the α dependence of the charge order signal is the new information that allows testing – through comparison with theoretical predictions from scattering theory – the validity of the scenarios under consideration for the symmetry of the CDW or-

der parameter. The azimuthal dependence of the REXS signal was studied in Bi2201-UD15K and in two underdoped $\text{YBa}_2\text{Cu}_3\text{O}_y$ compounds ($\text{YBa}_2\text{Cu}_3\text{O}_{6.51}$, YBCO-Ortho II, with $p \simeq 0.10$ and $\text{YBa}_2\text{Cu}_3\text{O}_{6.75}$, YBCO-Ortho III, with $p \simeq 0.13$; see also Materials and Methods). A series of in-plane momentum (Q_{\parallel}) scans of the charge order peak in YBCO-Ortho III is presented in Fig. 3c for the range $0^\circ < \alpha < 180^\circ$ and both σ - and π -polarized incoming X-rays.

The total scattered intensity I_{REXS} is extracted by fitting the REXS momentum scans with a Gaussian peak, and is in general proportional to the amplitude of the charge modulation. We can directly compare I_{REXS} to the theoretical REXS cross section [37, 38]:

$$I_{\epsilon \rightarrow \epsilon'}(\alpha) \propto \left| \sum_n e^{i\mathbf{Q}^* \cdot \mathbf{R}_n} \left(\sum_{pq} \epsilon_p \cdot F_{pq}^{(n)}(\omega, \alpha) \cdot \epsilon'_q \right) \right|^2, \quad (1)$$

where ϵ and ϵ' represent the polarization vectors for incoming and outgoing photons, respectively; \mathbf{Q}^* is the ordering wavevector; \mathbf{R}_n are the Cu lattice sites. $F_{pq}^{(n)}$ is the scattering tensor – dependent on photon energy (ω), azimuthal angle (α), and lattice site (n) – which in this case is diagonal ($F_{pq} = F_{pp}\delta_{pq}$). For a single Cu- $2p \rightarrow 3d$ transition within a CuO_2 plane, $F_{pq}^{(n)}$ is also well-approximated by a single Lorentzian peak with site- and orbital-dependent transition energies: $F_{pp}^{(n)}(\omega) \sim F_{pp}(\alpha) \times (\omega - \Delta E_p^{(n)} + i\Gamma)^{-1}$ (see Supplementary Information for a more detailed discussion). The total calculated scattering intensity is then given by: $I_{\text{calc}}(\alpha) = I_{\epsilon \rightarrow \sigma'}(\alpha) + I_{\epsilon \rightarrow \pi'}(\alpha)$, where $\epsilon = \sigma$ or π . In order to eliminate all possible extrinsic effects due to the sample shape and orientation with respect to the scattering

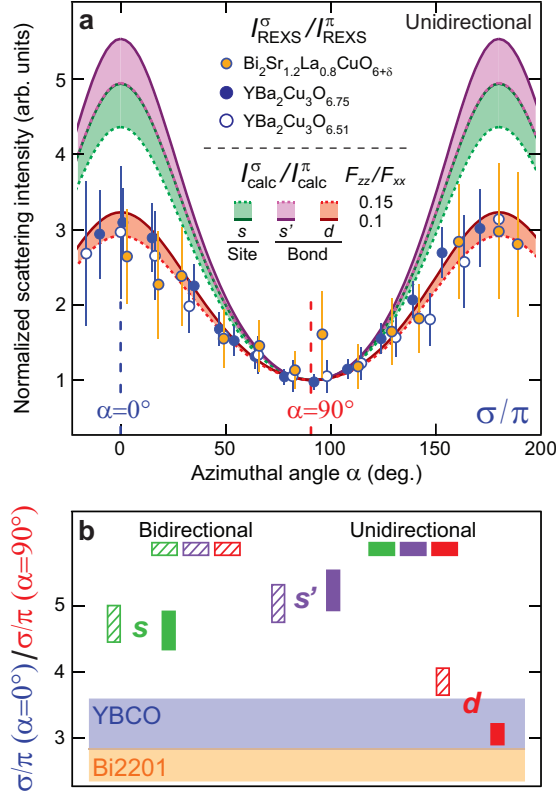


FIG. 4: **a**, Ratio of σ - to π -incident X-ray scattering intensity from CDW order in YBCO-OrthoII, YBCO-OrthoIII, and Bi2201-UD15K. Continuous lines represent the azimuthal angle-dependent scattering ratio $I^\sigma_{\text{calc}}/I^\pi_{\text{calc}}$ as calculated for the various symmetries of a unidirectional CDW order parameter (shaded areas cover the experimental range $0.1 < F_{zz}/F_{xx} < 0.15$); the curves are normalized at their minimum value (at $\alpha = 90^\circ$), which is set equal to 1. **b**, Ratio of the σ/π normalized scattering intensity between $\alpha = 0^\circ$ and $\alpha = 90^\circ$: colored boxes represent the ranges spanned by $I^\sigma_{\text{calc}}/I^\pi_{\text{calc}}$, while the bottom rectangles cover the experimental range for YBCO and Bi2201 as shown in **a**.

geometry (and thus facilitate the comparison to the theoretical predictions), we plot in In Fig. 4a the azimuthal dependence of the ratio $I^\sigma_{\text{REXS}}/I^\pi_{\text{REXS}}$ between the scattering intensity for σ - and π -polarized incident X-rays. Markers indicate experimental points (I_{REXS}), while continuous lines are model calculations (I_{calc}) for each separate term in the expansion of the CDW order parameter $\Delta_{\text{CDW}}(\mathbf{k}, \mathbf{Q})$. Here a unidirectional modulation is used, but the results are similar if a bidirectional order is assumed instead (see Supplementary Figure 2). The ratio F_{zz}/F_{xx} ($= F_{zz}/F_{yy}$) between those components of the diagonal scattering tensor controlling the out-of-plane (F_{zz}) and in-plane (F_{xx}) transition amplitudes is constrained to the range estimated from the X-ray absorption data (see Supplementary Information), corresponding to $F_{zz}/F_{xx} \sim 0.1-0.15$. Figure 4b compares the total amplitude of the I^σ/I^π profiles from Fig. 4a, as evaluated by taking the ratio between its $\alpha=0^\circ$ and $\alpha=90^\circ$

value, and highlights how the best overall agreement is achieved for a d -wave bond order.

In order to quantitatively assess the validity of these models, we have calculated the reduced chi-square (χ^2_{red}) for all the experimental points (inclusive of YBCO-OrthoII, YBCO-OrthoIII, and Bi2201-UD15K) and theoretical configurations shown in Fig. 4 (see Supplementary Information for a formal definition of χ^2_{red}). The values of χ^2_{red} are subsequently used to extract the probability P for the different models considered here. These probability levels (Table I) indicate that a d -wave bond-order is substantially more likely to describe the experimental data than site- or s -wave bond-orders, with the latter one being particularly inadequate. We note that the hierarchy in the likelihood of the various terms for the CDW order parameter seem to follow theoretical predictions for Δ_{CDW} in the context of the t - J model [25, 39, 40]. In addition, at this stage, the small difference between the probability level for bi- and uni-directional CDW does not allow us to conclusively establish which one better describes the experimental data.

Δ_{CDW}	Probability levels P (%)	
	Bidirectional	Unidirectional
Δ_s	30.3	38.8
$\Delta_{s'}(\cos k_x + \cos k_y)$	12.0	6.0
$\Delta_d(\cos k_x - \cos k_y)$	81.8	87.6

TABLE I: **Statistical comparison of CDW models.** Probability levels P for the hypothesis that a specific CDW model fits the experimental data better than a random sample. The values suggest that a d -wave bond-order state outperforms the other models in that it has a substantially greater likelihood of describing the experimental data. A uni- or bi-directional order describe the data equally well, as indicated by the proximity in their probability levels.

Altogether, we reveal the charge-ordered electronic ground state in two cuprate families to be best described by a d -wave bond-order with O-2 p charge modulations propagating exclusively along the **a** and **b** axes. Therefore, our study reaffirms the pivotal role played by the O-2 p ligand states [41, 42]. In light of recent results demonstrating the ubiquity of charge ordering in cuprates [21, 22], and of previous works pointing to bond-order in $\text{La}_{1.875}\text{Ba}_{0.125}\text{CuO}_4$ [6], $\text{Ca}_{1.88}\text{Na}_{0.12}\text{CuO}_2\text{Cl}_2$, and $\text{Bi}_2\text{Sr}_2\text{Dy}_{0.2}\text{Ca}_{0.8}\text{Cu}_2\text{O}_{8+\delta}$ [43, 44], we propose that the microscopic defining symmetry of such state is also universal, and of d -wave bond-order type. The commonality between the symmetry of the superconducting (SC) and CDW order parameters further suggests that the same attractive interaction responsible for particle-particle (Cooper) pairing and leading to the SC instability, might also be active in the particle-hole channel. This aspect – which has been recently proposed at the theoretical level and has been suggested to originate

from the exchange part (J) of the interaction Hamiltonian [25, 26, 39, 40] – is here corroborated by our experiments. This has deep implications in the context of the competing instabilities of the electronic system and for the ultimate understanding of the pairing mechanism.

* Electronic address: rcomin@physics.ubc.ca

† Electronic address: damascelli@physics.ubc.ca

- [1] H. Yoshizawa, H. Kawano, Y. Tomioka, and Y. Tokura, *Phys. Rev. B* **52**, R13145 (1995).
- [2] J. M. Tranquada, D. J. Buttrey, and V. Sachan, *Phys. Rev. B* **54**, 12318 (1996).
- [3] M. Cwik, M. Benomar, T. Finger, Y. Sidis, D. Senff, M. Reuther, T. Lorenz, and M. Braden, *Phys. Rev. Lett.* **102**, 057201 (2009).
- [4] J. M. Tranquada, B. J. Sternlieb, J. D. Axe, Y. Nakamura, and S. Uchida, *Nature* **375**, 561 (1995).
- [5] M. v. Zimmermann, A. Vigliante, T. Niemller, N. Ichikawa, T. Frello, J. Madsen, P. Wochner, S. Uchida, N. Andersen, J. M. Tranquada, et al., *Europhys. Lett.* **41**, 629 (1998).
- [6] P. Abbamonte, A. Rusydi, S. Smadici, G. D. Gu, G. A. Sawatzky, and D. L. Feng, *Nat. Phys.* **1**, 155 (2005), ISSN 1745-2473.
- [7] J. Fink, E. Schierle, E. Weschke, J. Geck, D. Hawthorn, V. Soltwisch, H. Wadati, H.-H. Wu, H. A. Dürr, N. Wient, et al., *Phys. Rev. B* **79**, 100502 (2009).
- [8] D. Poilblanc and T. M. Rice, *Phys. Rev. B* **39**, 9749 (1989).
- [9] J. Zaanen and O. Gunnarsson, *Phys. Rev. B* **40**, 7391 (1989).
- [10] K. Machida, *Physica C: Superconductivity* **158**, 192 (1989).
- [11] V. J. Emery, S. A. Kivelson, and H. Q. Lin, *Phys. Rev. Lett.* **64**, 475 (1990).
- [12] J. E. Hoffman, E. W. Hudson, K. M. Lang, V. Madhavan, H. Eisaki, S. Uchida, and J. C. Davis, *Science* **295**, 466 (2002).
- [13] C. Howald, H. Eisaki, N. Kaneko, and A. Kapitulnik, *Proc. Natl. Acad. Sci. U.S.A.* **100**, 9705 (2003).
- [14] T. Wu, H. Mayaffre, S. Kramer, M. Horvatic, C. Berthier, W. N. Hardy, R. Liang, D. A. Bonn, and M.-H. Julien, *Nature* **477**, 191 (2011).
- [15] G. Ghiringhelli, M. Le Tacon, M. Minola, S. Blanco-Canosa, C. Mazzoli, N. B. Brookes, G. M. De Luca, A. Frano, D. G. Hawthorn, F. He, et al., *Science* **337**, 821 (2012).
- [16] J. Chang, E. Blackburn, A. T. Holmes, N. B. Christensen, J. Larsen, J. Mesot, R. Liang, D. A. Bonn, H. W. N., A. Watenphul, et al., *Nat. Phys.* **8**, 871 (2012), ISSN 1745-2473.
- [17] A. J. Achkar, R. Sutarto, X. Mao, F. He, A. Frano, S. Blanco-Canosa, M. Le Tacon, G. Ghiringhelli, L. Braicovich, M. Minola, et al., *Phys. Rev. Lett.* **109**, 167001 (2012).
- [18] E. Blackburn, J. Chang, M. Hücker, A. T. Holmes, N. B. Christensen, R. Liang, D. A. Bonn, W. N. Hardy, U. Rütt, O. Gutowski, et al., *Phys. Rev. Lett.* **110**, 137004 (2013).
- [19] S. Blanco-Canosa, A. Frano, T. Loew, Y. Lu, J. Porras, G. Ghiringhelli, M. Minola, C. Mazzoli, L. Braicovich, E. Schierle, et al., *Phys. Rev. Lett.* **110**, 187001 (2013).
- [20] M. Le Tacon, A. Bosak, S. M. Souliou, G. Dellea, T. Loew, R. Heid, K.-P. Bohnen, G. Ghiringhelli, M. Krisch, and B. Keimer, *Nat. Phys.* **10**, 52 (2014).
- [21] R. Comin, A. Frano, M. Yee, Y. Yoshida, H. Eisaki, E. Schierle, E. Weschke, R. Sutarto, F. He, A. Soumyanarayanan, et al., *Science* **343**, 390 (2014).
- [22] E. da Silva Neto, P. Aynajian, A. Frano, R. Comin, E. Schierle, E. Weschke, A. Gyénis, J. Wen, J. Schneeloch, Z. Xu, et al., *Science* **343**, 393 (2014).
- [23] S. A. Kivelson, I. P. Bindloss, E. Fradkin, V. Oganessian, J. M. Tranquada, A. Kapitulnik, and C. Howald, *Rev. Mod. Phys.* **75**, 1201 (2003).
- [24] K. B. Efetov, H. Meier, and C. Pépin, *Nat. Phys.* **9**, 442 (2013).
- [25] S. Sachdev and R. La Placa, *Phys. Rev. Lett.* **111**, 027202 (2013).
- [26] J. C. S. Davis and D.-H. Lee, *Proc. Natl. Acad. Sci.* (2013).
- [27] H. Meier, M. Einenkel, C. Pépin, and K. B. Efetov, *Phys. Rev. B* **88**, 020506 (2013).
- [28] Y. He, P. Scherpelz, and K. Levin, *Phys. Rev. B* **88**, 064516 (2013).
- [29] S. Bulut, W. A. Atkinson, and A. P. Kampf, *Phys. Rev. B* **88**, 155132 (2013).
- [30] L. Nie, G. Tarjus, and S. A. Kivelson, *arXiv:1311.5580* (2013).
- [31] E. G. Dalla Torre, Y. He, D. Benjamin, and E. Demler, *arXiv:1312.0616* (2013).
- [32] P. Lee, *arXiv:1401.0519* (2014).
- [33] Y. Wang and A. Chubukov, *arXiv:1401.0712* (2014).
- [34] A. Melikyan and M. R. Norman, *Phys. Rev. B* **89**, 024507 (2014).
- [35] A. J. Achkar, F. He, R. Sutarto, J. Geck, H. Zhang, Y.-J. Kim, , and D. G. Hawthorn, *Phys. Rev. Lett.* **110**, 017001 (2013).
- [36] K. McElroy, J. Lee, J. A. Slezak, D.-H. Lee, H. Eisaki, S. Uchida, and J. C. Davis, *Science* **309**, 1048 (2005).
- [37] C. Schüßler-Langeheine, J. Schlappa, A. Tanaka, Z. Hu, C. F. Chang, E. Schierle, M. Benomar, H. Ott, E. Weschke, G. Kaindl, et al., *Phys. Rev. Lett.* **95**, 156402 (2005).
- [38] S. D. Matteo, *Journal of Physics D: Applied Physics* **45**, 163001 (2012).
- [39] M. Vojta and O. Rösch, *Phys. Rev. B* **77**, 094504 (2008).
- [40] M. A. Metlitski and S. Sachdev, *Phys. Rev. B* **82**, 075128 (2010).
- [41] J. Zaanen, G. A. Sawatzky, and J. W. Allen, *Phys. Rev. Lett.* **55**, 418 (1985).
- [42] V. J. Emery and G. Reiter, *Phys. Rev. B* **41**, 7247 (1990).
- [43] Y. Kohsaka, C. Taylor, K. Fujita, A. Schmidt, C. Lupien, T. Hanaguri, M. Azuma, M. Takano, H. Eisaki, H. Takagi, et al., *Science* **315**, 1380 (2007).
- [44] M. J. Lawler, K. Fujita, J. Lee, A. R. Schmidt, Y. Kohsaka, C. K. Kim, H. Eisaki, S. Uchida, J. C. Davis, J. P. Sethna, et al., *Nature* **466**, 347 (2010).

Acknowledgments

We are grateful to Yang He and M. Yee for sharing

the STM data shown in the manuscript. We also acknowledge E. Dalla Torre, J.C. Davis, E. Demler, D.G. Hawthorn, S.A. Kivelson, M. Le Tacon, C. Pepin, and S. Sachdev for insightful discussions. This work was supported by the Max Planck – UBC Centre for Quantum Materials, the Killam, Alfred P. Sloan, Alexander von Humboldt, and NSERC’s Steacie Memorial Fellowships (A.D.), the Canada Research Chairs Program

(A.D., G.A.S.), NSERC, CFI, and CIFAR Quantum Materials. Part of the research described in this paper was performed at the Canadian Light Source, which is funded by the CFI, NSERC, NRC, CIHR, the Government of Saskatchewan, WD Canada, and the University of Saskatchewan. R.C. acknowledges the receipt of support from the CLS Graduate Student Travel Support Program.